JOURNAL OF IRON AND STEEL RESEARCH, INTERNATIONAL. 2015, 22(6): 534-542

Low Cycle Fatigue Behavior and Cyclic Softening of P92 Ferritic-martensitic Steel

Zhen ZHANG[1], Zheng-fei HU[1], Li-kun FAN[2], Bin WANG[2]

(1. School of Materials Science and Engineering, Tongji University, Shanghai 201804, China; 2. Shanghai Key Laboratory for Engineering Materials Application Evaluation, Shanghai Research Institute of Materials, Shanghai 200437, China)

Abstract: The low cycle fatigue (LCF) behavior of P92 martensitic steel was investigated under different controlled strain amplitudes at room and high temperatures (873 K). The cyclic stress responses at all temperatures and strain amplitudes exhibited obviously rapid softening behavior at the early stage of fatigue life, and there was no saturated stage at high temperature. The fracture surfaces of the fatigue samples were observed by scanning electron microscopy (SEM) and optical microscopy. It was shown that crack initiation and propagation occurred transgranularly at both testing temperatures. A typical character was the high density crack branches or secondary cracks along fatigue striations at high temperature, which initiated from the oxidized inclusions and grain boundaries. Further investigation by transmission electron microscopy (TEM) showed that the softening behavior was attributed to the microstructure evolution during fatigue life, such as annihilation of dislocations and migration of martensite laths as well as carbide coarsening, especially for samples tested at high temperature.

Key words: low cycle fatigue; P92 steel; oxidative damage; cyclic softening

9%—12% Cr creep-resistant ferritic-martensitic steels possess high strength and high thermal conductivity, low thermal expansion, good corrosion resistance and good mechanical properties[1-3]. These characteristics make them extensively used as structural materials for the steam generator components and fossil fired power plants[4]. P92 steel is one of these 9%—12% Cr ferritic heat-resistant steels and its further increase in stress rupture strength is obtained by the addition of 1.8% W and the decrease of Mo content from 1% to 0.5%[5]. In earlier studies[6-9] on 9%—12% Cr steels, the major concerns have been focused on the enhancement of high temperature tensile strength and creep strength. Such improvements have been achieved by the variation of heat treatment[6,7] or by the addition of strong carbide formers such as Nb and V[7-9]. However, the components of the steam generators are often subjected to repeated thermal stresses as a result of temperature gradients that occur on heating and cooling during start-up and shutdown or during temperature transients. Therefore, failure mechanisms under such loading conditions are a result of complex interactions of creep and fatigue processes within low cycle fatigue (LCF) regime. The low cycle fatigue behavior of this kind of steel has been studied earlier under normalized and tempered[10-13] and thermally aged conditions[14,15]. However, the LCF behavior of P92 steel and the evolution of microstructure were not studied in detail. Park et al.[16] have studied the influence of W addition on the LCF resistance of the steel, and found that it increases with addition of W up to 1.8 mass% and decreases with further increase in W content. Giroux et al.[17] have studied the influence of strain rate on the microstructural stability and found that the lower the strain rate, the more pronounced the cyclic softening. In the following, the LCF behavior of P92 steel was studied. Some fatigue tests were carried out in air in constant strain at 873 K, a typical operating temperature of future components of fossil fired power plants. Others were carried out at room tem-

Foundation Item: Item Sponsored by Key Project of Shanghai Science and Technology Commission of China (10521100500)

Biography: Zhen ZHANG, Doctor; **E-mail**: 012zhangzhen@tongji.edu.cn; **Received Date**: February 24, 2014

Corresponding Author: Zheng-fei HU, Doctor, Professor; **E-mail**: huzhengf@tongji.edu.cn.

perature (RT) for comparison. Based on the test data, the crack propagation behavior in fatigue was identified and the correlation with microstructure evolution affecting cyclic softening was analyzed.

1 Experimental

1.1 Material

Fatigue tests were conducted on P92 steel specimens (Fig. 1) taken from the longitudinal direction of a commercial pipe. The chemical compositions specified by standard ASTM[18] and used in the tests are given in Table 1 and basic mechanical properties are given in Table 2. The initial microstructures of P92 steels are shown in Fig. 2. The normalizing and tempering treatment in steel resulted in a tempered martensite and the crystallographic structure is body centered cubic (BCC). The structure composed of martensite block, which consists of lath martensite decorated with stringers of $M_{23}C_6$ carbides that were Cr enriched at the lath boundaries, prior austenite grain boundaries and subgrain boundaries. In the intralath regions, fine MC type carbides rich in V and Nb

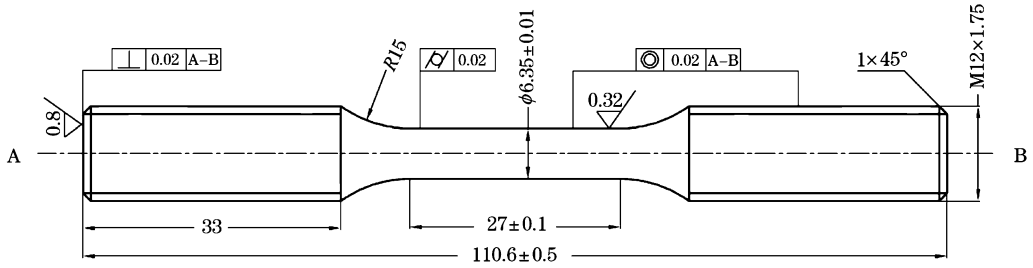

Fig. 1 Dimension of fatigue specimen (Unit: mm)

Table 1 Chemical composition of P92 steel mass%

	C	Mn	P	S	Si	Cr	W	Mo	V	Nb	N	B	Al	Ni
ASTM A335-2003	0.07—0.13	0.3—0.6	≤0.02	≤0.01	≤0.5	8.5—9.5	1.5—2.0	0.3—0.6	0.15—0.25	0.04—0.09	0.03—0.07	0.001—0.006	≤0.04	≤0.4
Test	0.1	0.45	0.015	0.008	0.3	8.82	1.57	0.35	0.2	0.078	0.037	0.0027	0.006	0.11

Table 2 Basic mechanical properties of P92 steel

Temperature/K	0.2% proof strength/MPa	Tensile strength/MPa	Reduction of area/%	Modulus of elasticity/GPa
RT	465	660	15	215
873	297	312	18	151

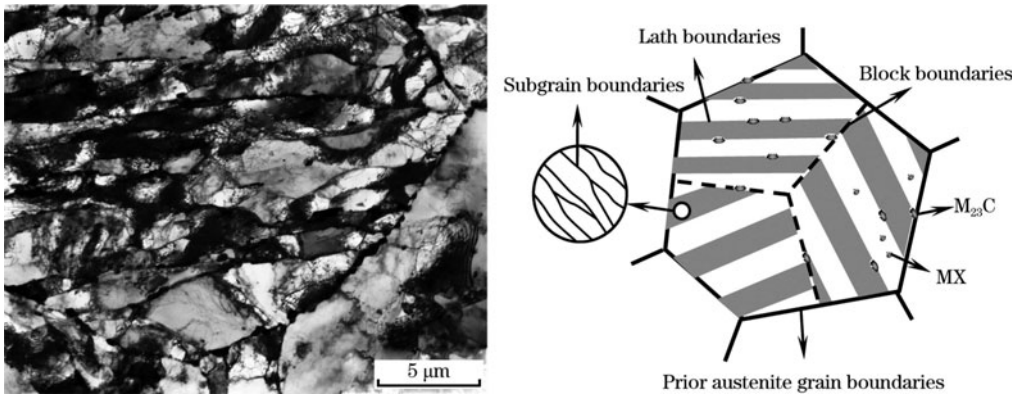

Fig. 2 Microstructure of tempered martensite and schematic diagram of P92 steel

were homogeneously dispersed[19].

1.2 Fatigue test

Fatigue tests at room temperature (RT) and 873 K were performed in tensile/compression conditions with asymmetry factor of $R=-1$. The tests were conducted in an MTS-809 testing machine under controlled strain at a constant strain rate of 0.004 s^{-1} at

different strain amplitudes. LCF life characteristics N_f was taken as the cycle number corresponding to a 20% drop in the peak tensile stress at half-life following the failure criterion proposed in literature[20]. The fatigue crack initiation and propagation behaviors under different testing conditions were studied by optical microscopy (OM) and scanning electron microscopy (SEM). Samples for the optical metallography were etched using Vilella′s reagent (1 g picric acid+5 mL HCl+100 mL ethyl alcohol) and examined under an optical microscope. The P92 steel shows a very high dislocation density after austenitizing, air cooling and tempering. The evolution of microstructure like martensite lath, dislocation and carbides was observed by transmission electron microscopy (TEM).

2 Results and Discussion

2.1 Cyclic properties

The material generally showed a continuous softening regime that ends in a period of stress saturation. The stress plateau continued till the onset of final load drop, which occurs due to the initiation and propagation of fatigue cracks. This type of softening behavior is known to occur in ferritic steels when the initial microstructure contains a lot of dislocations, which redistribute to have a low energy configuration[21] such as dislocation network, cell structure and slip deformation band during cyclic deformation or disappears by annihilation process[22]. The cyclic stress response of the steel under different strain amplitudes and temperature conditions is presented in Figs. 3 and 4. The maximum peak tensile stress for all curves was obtained during the first cycles, and then a large amount of softening from the first cycle onwards occurred, after which there was a gradual change in the stress values under all the test conditions. The stabilizing cycles and total life were significantly decreased with the increase in strain amplitude as shown in Fig. 3(a). However, at 873 K (Fig. 3(b)), the stress amplitude decreased continuously without showing any stabilized value in all strain amplitudes. When the stress is not stabilized during cycling, the hysteresis loop at half-life cycle is usually chosen to obtain the cyclic stress-strain curve[23].

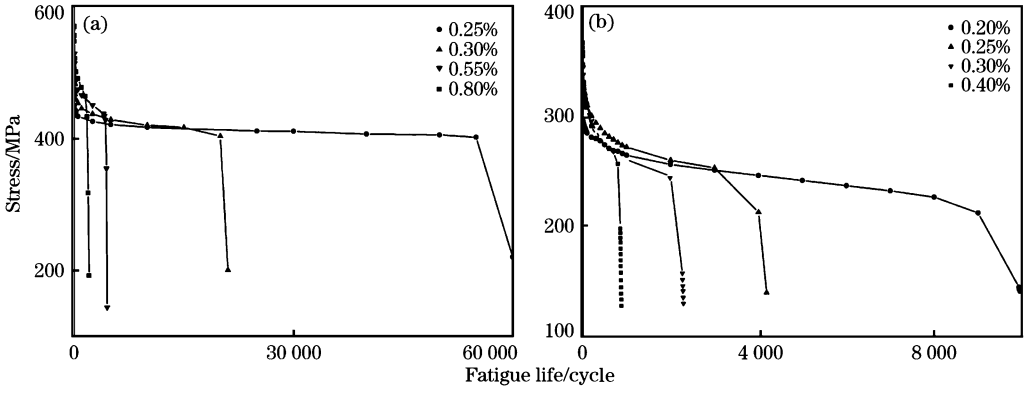

Fig. 3 Cyclic stress response curves at room temperature (a) and 873 K (b)

The cyclic stress response under different strain amplitudes was compared at two temperatures, as shown in Fig. 4. The amount of softening (As) incurred during cycling was calculated with respect to the first cycle stress as given in Eq. (1).

$$As(\%)=[(\sigma_i-\sigma_h)/\sigma_i]\times 100 \quad (1)$$

where σ_i and σ_h denote the peak tensile stress at the first cycle and at half-life, respectively. It was evident that the softening amount and rates (Fig. 3) were accelerated at high temperature, and the strain amplitude had no significant impact on this behavior. However, the softening rates (obtained from the slope in the linear portion of the log-log plot of cyclic stress response curses) were found to be similar in both vacuum and air under similar test conditions[24]. This indicated that the softening rate was independent of

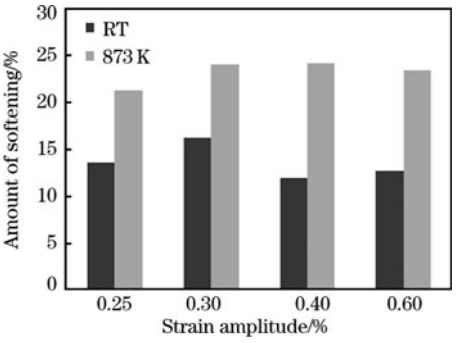

Fig. 4 Amount of softening for different test conditions

presence/absence of surface oxides and confirmed that the softening was caused by an internal phenomenon such as annihilation and rearrangements of dislocations and coarsening of strengthening carbides[25].

The cyclic stress-strain curves of the steel (corresponding to 1st cycle and half-life) at RT and 873 K are presented in Fig. 5, since the designers need these curves for a detailed inelastic analysis of the components. The half-life cyclic stress-strain curves at all temperatures could be represented by the well-known power law relationship

$$\frac{\Delta\sigma}{2}=K\left(\frac{\Delta\varepsilon_p}{2}\right)^n \tag{2}$$

where, K and n are the cyclic strain hardening coefficient and the cyclic strain hardening exponent, respectively. A tabulation of K and n values for the two temperatures is presented in Table 3. Although it is known that the values of n for metals are in the range between 0.1 and 0.2[26], the values in this work are smaller than 0.1 at both temperatures. The cyclic softening exhibited by the steel is reflected in these stress-strain curves. Several studies[27-29] showed that this softening behavior is due to an increase in size of the microstructure. Sauzay[30] also proposed a model based on destruction of the low-angle boundaries in order to predict coarsening of the matrix microstructure.

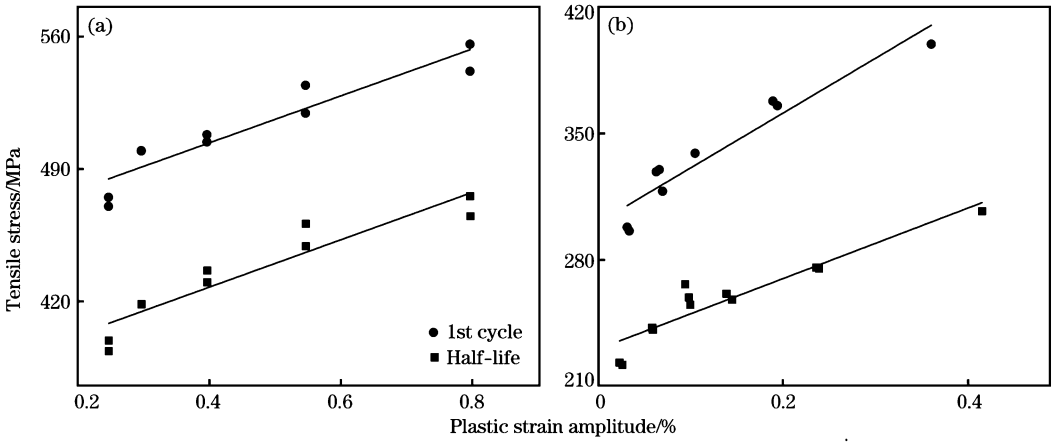

Fig. 5 Cyclic stress-strain curves plotted for different cycle numbers at room temperature (a) and 873 K (b)

Table 3 Constants in Manson-Coffin and Basquin relationships and cyclic stress-strain relationship of P92 steel at two temperatures

Temperature/K	σ'_f/MPa	ε'_f	b_0	c_0	K	n
RT	713.0	1.196	−0.04954	−0.6484	705.7	0.075
873	423.9	27.710	−0.07055	−0.6261	475.4	0.090

Note: ε'_f is the fatigue strength coefficient; b_0 is the fatigue strength exponent; σ'_f is the fatigue ductility coefficient; c_0 is the fatigue ductility exponent.

2.2 Fatigue life and damage

The fatigue life at high temperature was greatly reduced compared with that at RT (Fig. 6). The amount of reduction was remarkable at low strain amplitude implying that other factors might also affect the fatigue crack initiation and propagation processes. The fatigue lives at all temperatures have been found to follow the strain-life relationship derived by Raske and Morrow[26] and Landgraf et al.[31] based on the relationship proposed by Basquin[32], Coffin[33] and Manson[34]. The strain-life relationship is given by

$$\frac{\Delta\varepsilon_t}{2}=\frac{\sigma'_f}{E}(2N_f)^{b_0}+\varepsilon'_f(2N_f)^{c_0} \tag{3}$$

where, $\Delta\varepsilon_t/2$ is the total strain amplitude; $2N_f$ is the number of reversals to failure; and E is the elastic modulus. The values of these constants and coef-

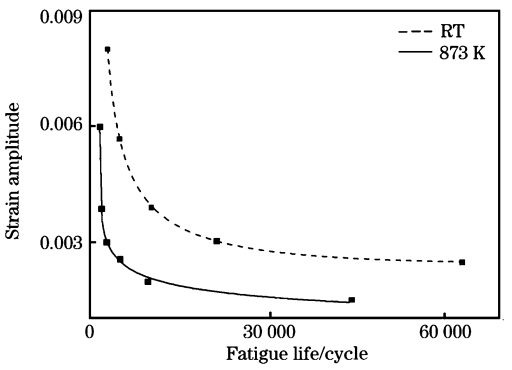

Fig. 6 Coffin-Manson plots at different temperatures

ficients for Eq. (3) established by least-square analysis are summarized in Table 3 for the two temperatures investigated. In general, c_0 is in the range between -0.5 and -0.7 for ductile materials[26] and the present values fit well at both temperatures.

The steel exhibited an increase in fatigue damage at high temperature and the effect of temperature on fatigue damage was more pronounced at the end of fatigue life, as seen in the fatigue damage with cycle life fraction N/N_f(Fig. 7). This is attributed to the fact that oxidation at high temperature plays an important role in fatigue damage[24]. The fatigue damages at the two temperatures have been found to follow the non-linear continuous fatigue damage model derived by Lemaitre and Chaboche[35]. The damage model is given by

$$D=1-\left\{1-\frac{N}{N_f\Delta\varepsilon_t}\left[1-(1-D_c)^{\alpha+1}\right]\right\}^{1/(\alpha+1)} \quad (4)$$

where, D is the damage; α is the temperature-dependent coefficient; and D_c is the damage when $N=N_f$.

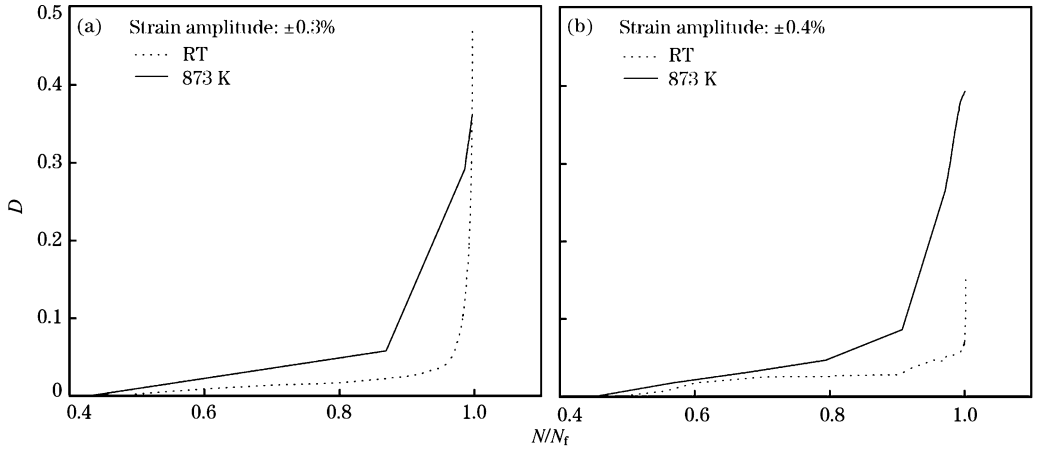

Fig. 7 Influence of cycle life fraction on the LCF damage at different strain amplitudes and temperatures

2.3 Crack propagation and fracture behavior

Fig. 8 shows the fracture surfaces of P92 steel at RT and high temperatures. Several fatigue sources lied in the margin of fracture surface at the strain amplitude of 0.6%. The cracks initiated from the grain boundaries which were linked with sample surface (Fig. 8(a)) and inclusions near the surface (Fig. 8(b)). It could be seen that significant fatigue cracks initiated from the surface and propagated gradually to the inner at high temperature. Fatigue striations and secondary cracks perpendicular to crack propagation direction were observed clearly in fracture surfaces, especially at high temperature. The secondary cracks and oxide layers were frequently observed at high temperature, which was considered important in reducing the LCF resistance[16]. Oxide layers initially formed on the surface (i.e., on the surface of slip band intrusion and extrusion) could easily penetrate into specimen interior during fatigue loading. Oxide film ruptured at crack tip or enhanced slip irreversibility is the possible mechanisms for the life reduction[36]. Fig. 8(e) shows the EDS analysis of the field around the crack at the extension zone at high temperature. Fig. 8(f), by contrast, shows the EDS analysis of the field at the final rupture zone of the same sample. It was observed that the oxygen content was higher at the extension zone than that at the rupture zone; thus, the existence of oxide layers and the oxidative damage during fatigue life could be proved.

The optical micrographs of longitudinal sections of P92 steel after fatigue fracture are shown in Fig. 9. Extensive branching of transgranular secondary cracks, with length varying from 50 to 70 μm, were clearly observed near surface at high temperature (Fig. 9(b)), but there were no obvious secondary cracks at RT (Fig. 9(a)). The higher density crack branches or secondary cracks along fatigue striations at high temperature indicated much wider plastic deformation close to the main crack facets. In Fig. 9(c), it could be seen that secondary cracks linked with inclusions. The secondary cracks would initiate from the interface of matrix and inclusions when the main crack extended to inclusions[37]. It could also be seen that secondary cracks paralleled with fatigue strips in Fig. 8, which may be due to the brittle grain boundaries. The grain boundary would be firstly oxidized and became brittle during fatigue at high temperature. Then, secondary cracks would initiate from these sites when the main crack

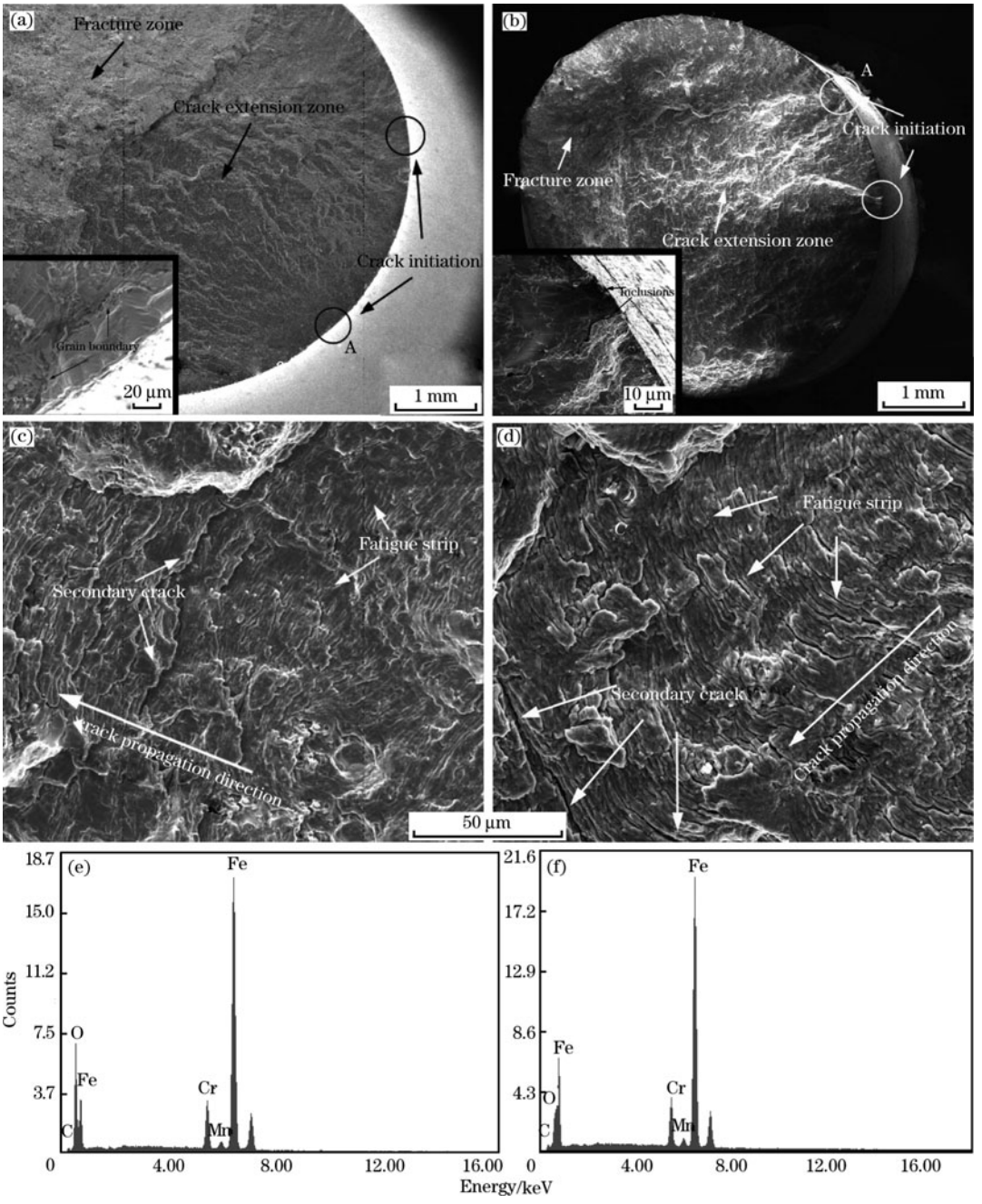

(a), (c) RT; (b), (d), (e), (f) 873 K.

Fig. 8 Fractographs of fracture surfaces of P92 steel at the strain amplitude of ±0.60%

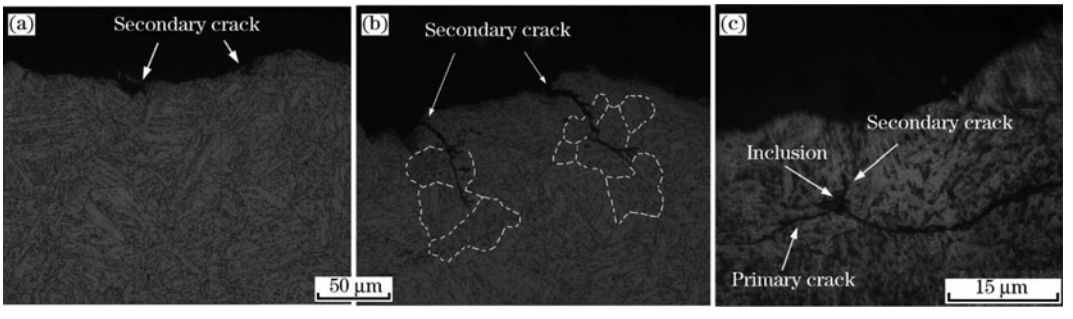

(a) RT; (b), (c) 873 K.

Fig. 9 Optical micrograph of the secondary crack propagation at the strain amplitude of ±0.15%

extended to these brittle boundaries. Due to the oxidized inclusions and grain boundaries during fatigue life, the secondary cracks initiated easily and propagated to the inner at high temperature.

2.4 Microstructure evolution

Previous investigations[38] reported that continuous cycling produces changes in the microstructure and a marked cyclic softening. Giroux et al.[17] studied this kind of steel and showed that the softening mechanisms are based on the annihilation of subgrain boundaries and mobile dislocations. Since the early work of Cottrell[39] and others[40,41], it is assumed that the flow stress to produce plastic deformation during cyclic test is composed of two contributions: the short distance interaction stress named friction stress σ_f, and the long distance interaction stress named back stress σ_b. The friction stress depends on the short-range obstacles that the initial internal structure of the material imposes to the dislocation movement, such as the lattice friction, precipitated particles, other dislocations and foreign atoms. On the other hand, the back stress depends on the density of long-range impenetrable obstacles such as subgrain boundaries[42]. The following equations show the relationships of σ_f and σ_b to the maximum peak tensile stress σ_{max} and yield stress σ_y,

$$\sigma_f = \frac{1}{2}(\sigma_{max} + \sigma_y) \tag{5}$$

$$\sigma_b = \frac{1}{2}(\sigma_{max} - \sigma_y) \tag{6}$$

Fig. 10 shows the evolution of the peak tensile stress, the friction stress and back stress presented at RT and 873 K, both using a total strain amplitude of 0.4%. As can be seen, the cyclic stress amplitude shows a continuous softening behavior up to fracture, which is much more pronounced for the first cycle at the two temperatures. After a very short consolidation phase for the first cycle, the cyclic stress amplitude decreases rapidly. At RT, a quasi-saturation stress level is reached after the rapid softening stage; however, the cyclic stress decreases slowly, without reaching a saturation stage after the rapid softening stage at 873 K. The friction stress depends on the short-range obstacles that the initial internal structure of the material imposes to the dislocation movement. Therefore, the decrease of the friction during cycling can be due to a decrement on the free dislocation density inside subgrains. On the other hand, the back stress depends on the density of long-range impenetrable obstacles such as subgrain boundaries. The decrease of the back stress can be attributed to the partial annihilation of these boundaries such as the coarsening of martensite laths. The friction stress exhibits a pronounced cyclic decrease at the beginning of the fatigue life at both RT and 873 K, which can be due to the rearrangement of dislocation and the decrement of dislocation density. It shows that the softening behavior at the beginning of fatigue life is mainly affected by the movement of dislocation for samples at both temperatures. As cycling proceeds, the friction stress curves at both temperatures show similar softening behavior as the peak tensile stress curve but the back stress curve at high temperature exhibits a slow cyclic decrease that lasts up to rupture, which can be attributed to the annihilation of boundaries. The softening behavior at high temperature is affected by these two factors, including the annihilation of dislocations and lath boundaries. On the other hand, the softening behavior at RT is mainly affected by the processes taking place inside the subgrains, such as annihilating dislocations.

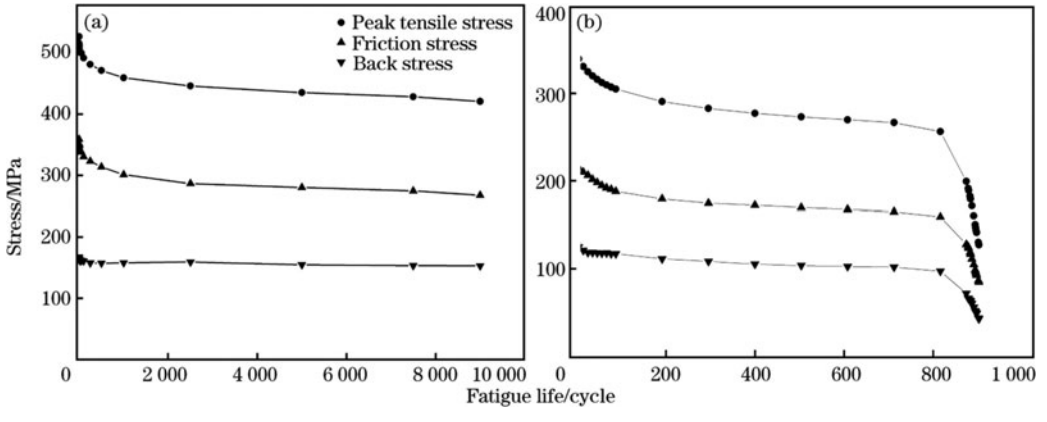

(a) RT; (b) 873 K.

Fig. 10 Evolution of the tensile stress, the friction stress and back stress presented with strain range of 0.4%

Figs. 11(a) to 11(d) shows the characteristic microstructures for samples fatigued with a total strain amplitude of 0.4% at RT and 873 K up to rupture. It shows that cycling in constant strain range induces visible microstructure evolutions. Compared with the original microstructure in Fig. 2, the apparently stable lath martensite structure is strongly unstable under cyclic conditions being gradually replaced by the development of subgrains and the free dislocation density located in the interior of the subgrains showed a significant decline (Figs. 11(a) and 11(b)). Nevertheless, some dislocations could also be observed mainly in small subgrains, suspected not to be deformed plastically, or inside subgrains in which they were pinned by carbides. Compared with sample tested at RT, the growth of subgrains (Fig. 11(b)) and the annihilation of lath boundaries (Fig. 11(d)) are observed, which suggests that the migration and annihilation of lath boundaries occur during cycling. The presence of carbides inside the subgrains which are lined up indicates the position of prior laths boundaries that completely disappeared during cycling (Fig. 11(d)). It can also be found that some subgrain boundaries disappear during cycling, the relatively coarse $M_{23}C_6$ carbides and some carbides become spherical or coagulate with adjacent carbides (Fig. 11(c)). The rearrangement of dislocation and the decline of dislocation density at RT and high temperatures weaken the dislocation strengthening; meanwhile, the annihilation of lath boundaries and the coarse carbides at high temperature result in the decrease of strengthening by the laths and carbides. All these evolutions of microstructures lead to the cyclic softening in the fatigue and the more obvious cyclic softening at high temperature can also be explained. Nevertheless, the interaction of carbides with dislocations in some subgrains can also be observed (Fig. 11(d)). The larger carbides (above 50 nm) were surrounded by tangled dislocation and the smaller carbides pinned dislocation, which all inhibited the cyclic softening and manifested as the decline of softening rates at the stress saturation stage[43].

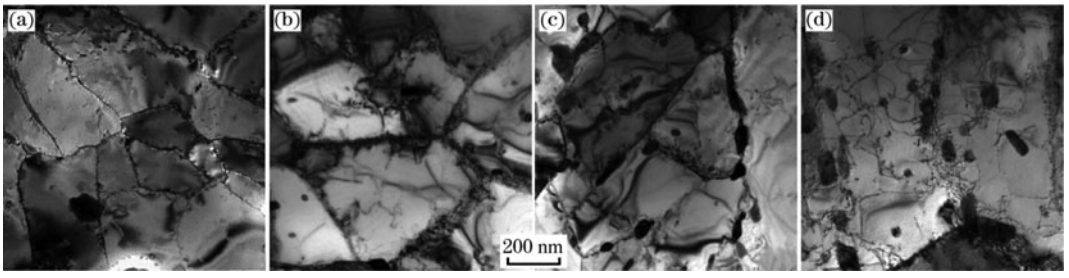

(a) RT, the evidence for subgrains and decline of dislocation density; (b) 873 K, the growth of subgrains and the dislocation moved toward subgrain boundaries as a rearrangement; (c) 873 K, the coarsening and joining of carbides; (d) 873 K, aligned carbides depict the position of prior lath boundaries and the interaction of carbides with dislocations.

Fig. 11 Characteristic microstructures for samples fatigued using a plastic range of 0.4% at RT and 873 K up to rupture

3 Conclusions

(1) The fatigue life of P92 steel was found to decrease and the fatigue damage was found to increase at high temperature, which was marked by extensive crack branching and the formation of secondary cracks. The obvious crack branches or secondary cracks along fatigue striations at high temperature initiated from the oxidized inclusions and grain boundaries.

(2) P92 steel in normalized and tempered condition showed pronounced softening under LCF conditions at all temperatures and strain amplitudes investigated. The amount and rate of softening was found to increase at high temperature. The rapid softening at the beginning of fatigue life was mainly affected by the annihilation of dislocations at these two temperatures. The softening behavior at RT was mainly affected by the annihilation of dislocations taking place inside the subgrains, while the softening behavior at high temperature was attributed to the annihilation of dislocations and coarsening of martensite laths and carbides.

References:

[1] Y. Yi, B. Lee, J. Kim, J. Jang, Mater. Sci. Eng. A 429 (2006) 161-168.

[2] M. Toloczko, M. Hamilton, S. Maloy, J. Nucl. Mater. 318 (2003) 200-206.

[3] J. Henry, X. Averty, Y. Dai, P. Lamagnèrea, J. P. Pizzanellib, J. J. Espinasb, P. Widenta, J. Nucl. Mater. 318 (2003) 215-227.

[4] R. Kannan, V. S. Srinivasan, M. Valsan, K. Bhanu Sankara Rao, Trans. Indian Inst. Met. 63 (2010) 571-574.

[5] P. J. Ennis, A. Czyrska-Filemonowicz, Sadhana 28 (2003) 709-

730.
[6] H. D. Kim, I. S. Kim, ISIJ Int. 34 (1994) 198-204.
[7] W. J. Plumbridge, N. Knee, Mater. Sci. Technol. 1 (1985) 577-582.
[8] A. Vyrostkova, A. Kroupa, J. Janovec, M. Svoboda, Acta Mater. 46 (1998) 31-38.
[9] K. Hamada, K. Tokuno, Y. Tomita, H. Mabuchi, K. Okamoto, ISIJ Int. 35 (1995) 86-91.
[10] G. Ebi, A. J. McEvily, Fatigue Fract. Engg. Mater. Struct. 7 (1984) 299-314.
[11] R. W. Swindman, S. D. Solomon, G. R. Halford, L. R. Kaisand, B. N. Leis, Low Cycle Fatigue, ASTM STP 942, ASTM, Philadelphia, 1998.
[12] A. Nagesha, M. Valsan, R. Kannan, K. Bhanu Sankara Rao, S. L. Mannan, Int. J. Fatigue 24 (2002) 1285-1293.
[13] S. Nishino, K. Shiozawa, A. Kojima, S. Seo, Y. Yamamoto, J. Soc. Mat. Sci. Jaan 48 (1999) 610-615
[14] B. G. Gieseke, C. R. Brinkman, P. J. Maziasz, Microstructure and Mechanical Properties of Aging Material, Chicago, United State, 1993.
[15] H. Okamura, R. Ohtani, K. Saito, K. Kimurad, R. Ishiid, K. Fujiyamad, S. Hongod, T. Isekid, H. Uchidad, Nuclear Engineering and Design 193 (1999) 243-254.
[16] J. S. Park, S. J. Kim, C. S. Lee, Mater. Sci. Eng. A 298 (2001) 127-136.
[17] P. F. Giroux, F. Dalle, M. Sauzay, C. Caës, B. Fournier, T. Morgeneyer, A. F. Gourgues-Lorenzon, Procedia Engineering 2 (2010) 2141-2150.
[18] ASTM, Standard Specification for Seamless Ferritic Steel-Steel Pipe for High-temperature Service, US, A335, 2003.
[19] V. K. Sikka, C. T. Ward, K. C. Thomas, in: A. K. Khare (Eds.), Ferritic Steels for High Temperature Applications, Proceedings of ASM International Conference on Production, Fabrication, Properties and Application of Ferritic Steels for High Temperature Applications, American Society for Metals, Ohio, 1983. pp. 65-84.
[20] K. Bhanu Sankara Rao, M. Valsan, R. Sandhya, S. K. Ray, S. L. Mannan, P. Rodriguez, Int. J. Fatigue 7 (1985) 141-147.
[21] M. F. Giordana, I. Alvarez-Armas, M. Sauzay, A. F. Armas, Key Eng. Mater. 465 (2011) 358-361.
[22] D. M. Li, K. W. Kim, C. S. Lee, Int. J. Fatigue 19 (1997) 607-612.
[23] B. K. Choudhary, K. B. S. Rao, S. L. Mannan, Metall. Mater. Trans. A 30 (1999) 2825-2834.
[24] V. Shankar, V. Bauer, R. Sandhya, M. D. Mathew, H. J. Christ, J. Nuclear Mater. 420 (2012) 23-30.
[25] V. Shankar, M. Valsan, K. Bhanu Sankara Rao, Mater. Sci. Eng. A 437 (2006) 413-422.
[26] D. T. Raske, J. D. Morrow, Manual on Low Cycle Fatigue Testing, US, ASTM-STP465, 1969.
[27] G. Eggeler, N. Nilsvang, B. Ilschner, Steel Res. 58 (1987) 97-103.
[28] K. Sawada, M. Takeda, K. Maruyama, R. Ishii, M. Yamada, Y. Nagae, R. Komine, Mater. Sci. Eng. A 267 (1999) 19-25.
[29] E. Cerri, E. Evangelista, S. Spigarelli, P. Bianchi, Mater. Sci. Eng. A 245 (1998) 285-292.
[30] M. Sauzay, Mater. Sci. Eng. A 510-511 (2009) 74-80.
[31] R. W. Landgraf, J. Morrow, T. Endo, J. Mater. JMLSA 4 (1969) 176-188.
[32] O. H. Basquin, Proc. Am. Soc. Test Mater. ASTEA 10 (1910) 625-630.
[33] L. F. Coffin Jr, Trans. ASME 76 (1954) 931-950.
[34] S. S. Manson, Behaviour of Materials under Conditions of Thermal Stress, NACA Tech Note-2933, Cleveland, 1953.
[35] J. L. Chaboche, P. M. Lesne, Fatigue Fract. Engng. Mater. Struct. 11 (1988) 1-17.
[36] G. Ebi, A. J. McEvily, Fatigue Fract. Eng. Mater. Struct. 7 (1984) 299-314.
[37] Z. W. Huang, F. H. Yuan, Z. G. Wang, S. J. Zhu, F. G. Wang, Acta Metall. Sin. 43 (2007) 1025-1030.
[38] R. Kannan, V. S. Srinivasan, M. Valsan, K. Bhanu Sankara Rao, Trans. Indian Inst. Met. 63 (2010) 571-574.
[39] A. H. Cottrell, Dislocations and Plastic in Flow in Crystal, Oxford University Press, London, 1953.
[40] D. Kuhlmann-Wilsdorf, Mater. Sci. Eng. 37 (1979) 111-120.
[41] J. I. Dickson, J. Boutin, L. Handfield, Mater. Sci. Eng. 64 (1984) L7-L11.
[42] M. F. Giordana, I. Alvarez-Armas, A. Armas, J. Nucl. Mater. 424 (2012) 247-251.
[43] Q. X. Zhao, L. H. Zhu, H. C. Gu, Y. S. Lu, J. Power Eng. 25 (2005) s1, 120-125.